Sensor and Simulation Notes

Note 487

March 2004

A Solid Dielectric Lens Impulse Radiating Antenna Surrounded by a Cylindrical Shroud

Everett G. Farr, Lanney M. Atchley, and Donald E. Ellibee
Farr Research, Inc.

Larry L. Altgilbers
U.S. Army Space and Missile Defense Command

Abstract

We investigate here the Solid Dielectric Lens Impulse Radiating Antenna (SDL IRA), which will be suitable for Ultra-Wideband, high-voltage transmission from the front end of an electrically conducting cylindrical shroud. The design is similar to a TEM horn embedded in solid UHMW polyethylene, with a lens in the aperture at the air-dielectric interface, surrounded by an electrically conducting cylindrical shroud that is open at the end. We have taken steps to harden the antenna to both high voltages and high forces. We investigated the effect of using two different impedances for the TEM horn, and we found that the high-impedance version worked best. We also investigated the effect of the position of the conducting cylindrical shroud with respect to the antenna, and we found it important to push the antenna as far forward of the shroud as possible. Finally, we identified an optimal placement of the terminating resistors that reduces reflections back into the source. We observed a frequency range of 400 MHz to 8 GHz, but it could go as high as 20 GHz with further refinements.

Table of Contents

1. Introduction

We consider here high-voltage Ultra-Wideband (UWB) antennas that can fit into the open end of an electrically conducting cylindrical shroud. Our goal is to develop an antenna that can radiate as broad a bandwidth as possible with maximum gain and at maximum voltage. The antenna should also be rugged enough to tolerate high forces.

To address this problem, we designed and built the *Solid Dielectric Lens Impulse Radiating Antenna* (SDL IRA). This device consists of a TEM horn that is embedded in polyethylene, with a lens in the aperture at the air-dielectric interface. We had previously built similar devices for low-voltage applications that are somewhat larger [1,2]. In this investigation we refine the existing antenna to make it more suitable for mounting it within a cylindrical shroud. The refinements included strengthening the design for mechanical shock and high voltages, and reducing its size.

In this investigation we determine the effect of the TEM horn impedance, and the effect of the lens. We also optimize the placement of the terminating resistors, and we quantify the effect of the position of the conducting cylindrical shroud. We begin now with a summary of the antenna design.

2. Design

2.1 Physical Construction

We designed and fabricated two versions of the SDL IRA. The first version, shown in Figure 2.1, is a 50-ohm design for applications requiring low reflections and a matched impedance. The second version, shown in Figures 2.2 and 2.3, is a high-impedance design to maximize antenna gain, and to take maximum advantage of the available aperture area. (Note that Figure 2.3 is an early sketch, with a few details missing.) We show photographs of the completed antennas in Figure 2.4.

The TEM horn sections of both antennas are embedded in a dielectric cylinder with a diameter of 127 mm (5 inches). We used a standard 6-inch outer diameter aluminum tube with a 0.5-inch wall thickness. The aluminum tube is 30.5 cm (12 inches) long.

Both antennas are completely filled with dielectric material to avoid high-voltage breakdown. The dielectric material, ultra-high molecular weight (UHMW) polyethylene, surrounds the metallic elements providing both a higher dielectric constant than air, and a much higher dielectric strength. We intended that this solid design would be sturdy enough to sustain high forces.

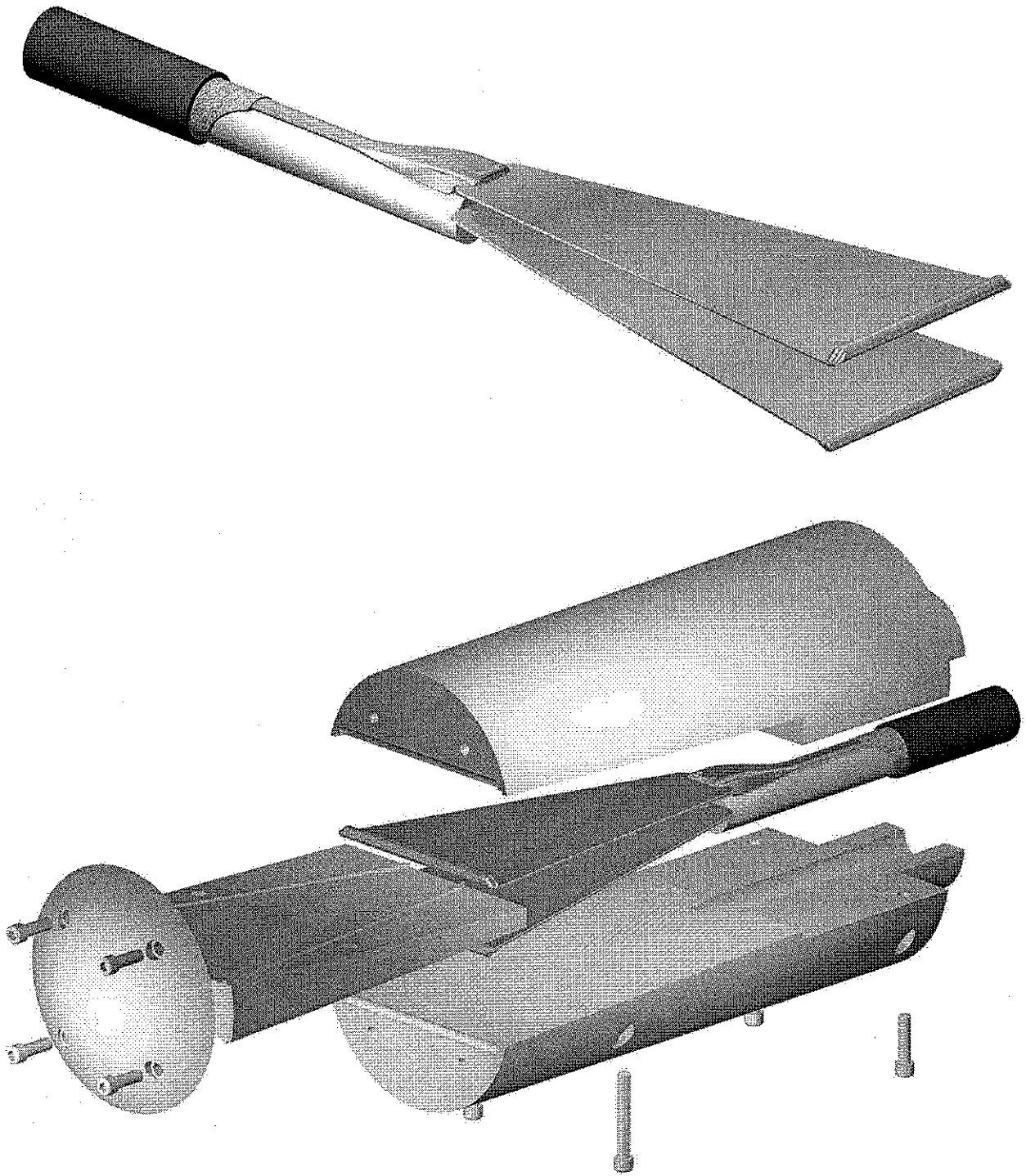

Figure 2.1. 50-ohm SDL IRA (top), exploded view with dielectric (bottom).

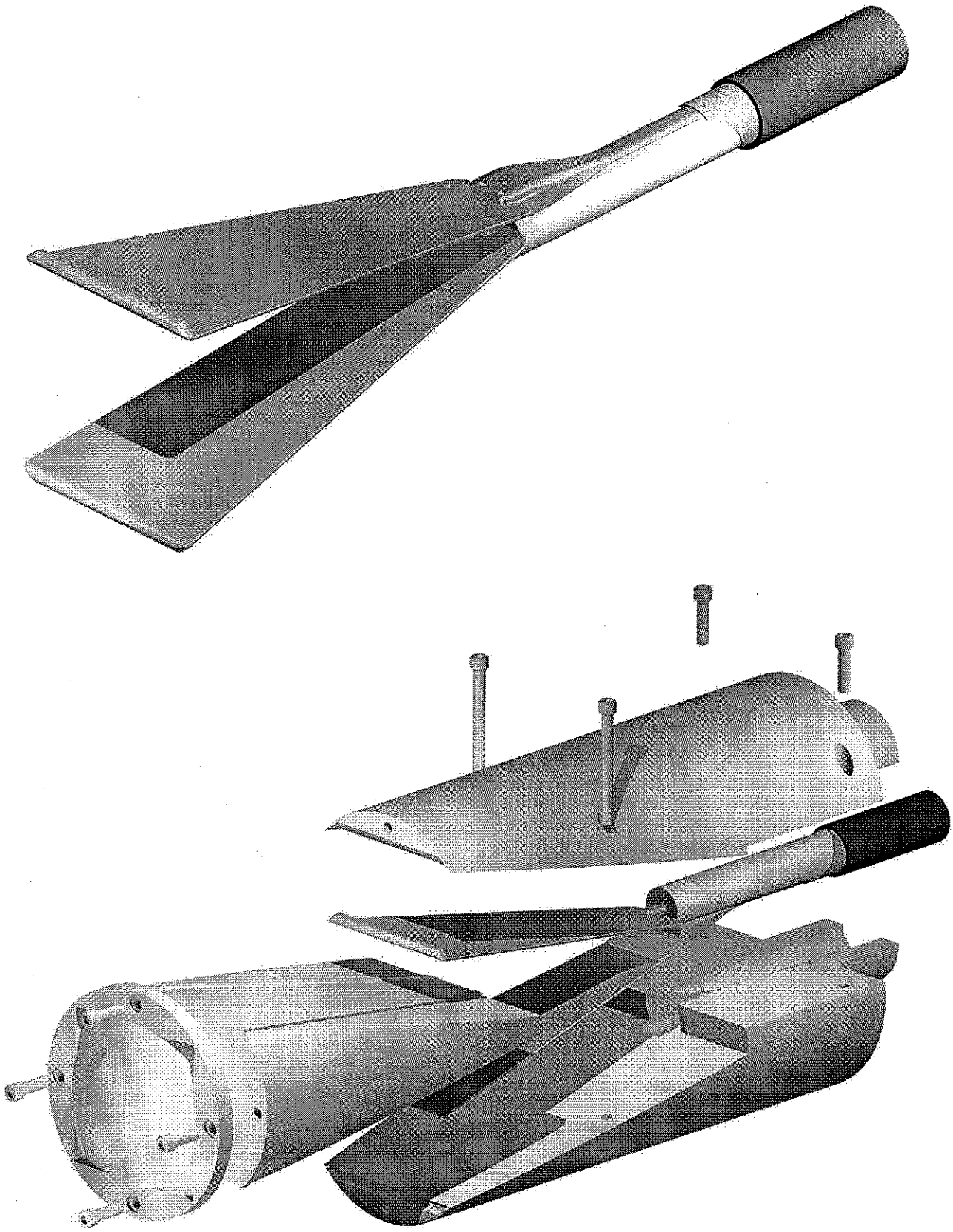

Figure 2.2. High impedance SDL IRA (top), exploded view with dielectric (bottom).

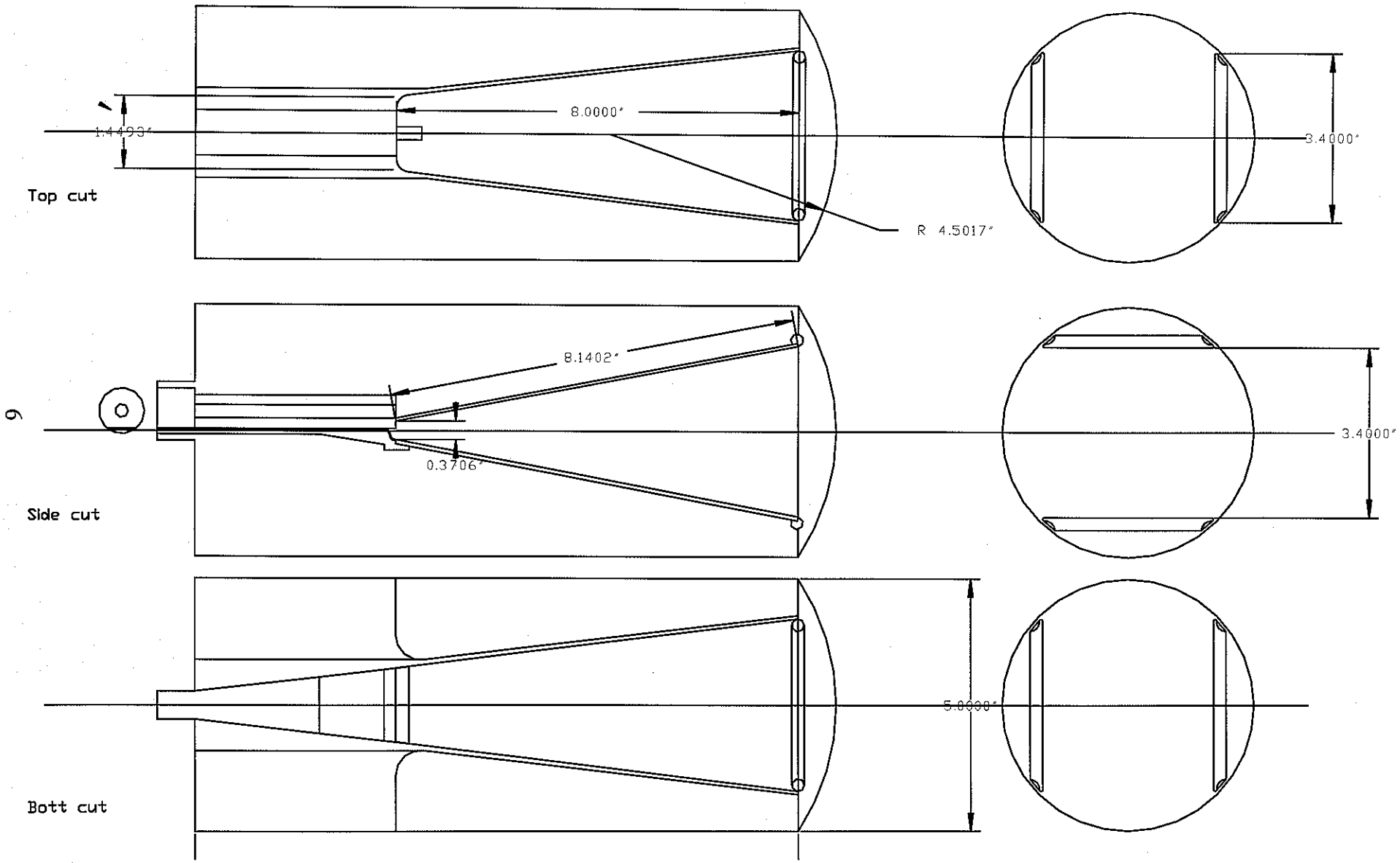

Figure 2.3. Early sketches of the High-Impedance version of the SDL IRA (some detail is missing).

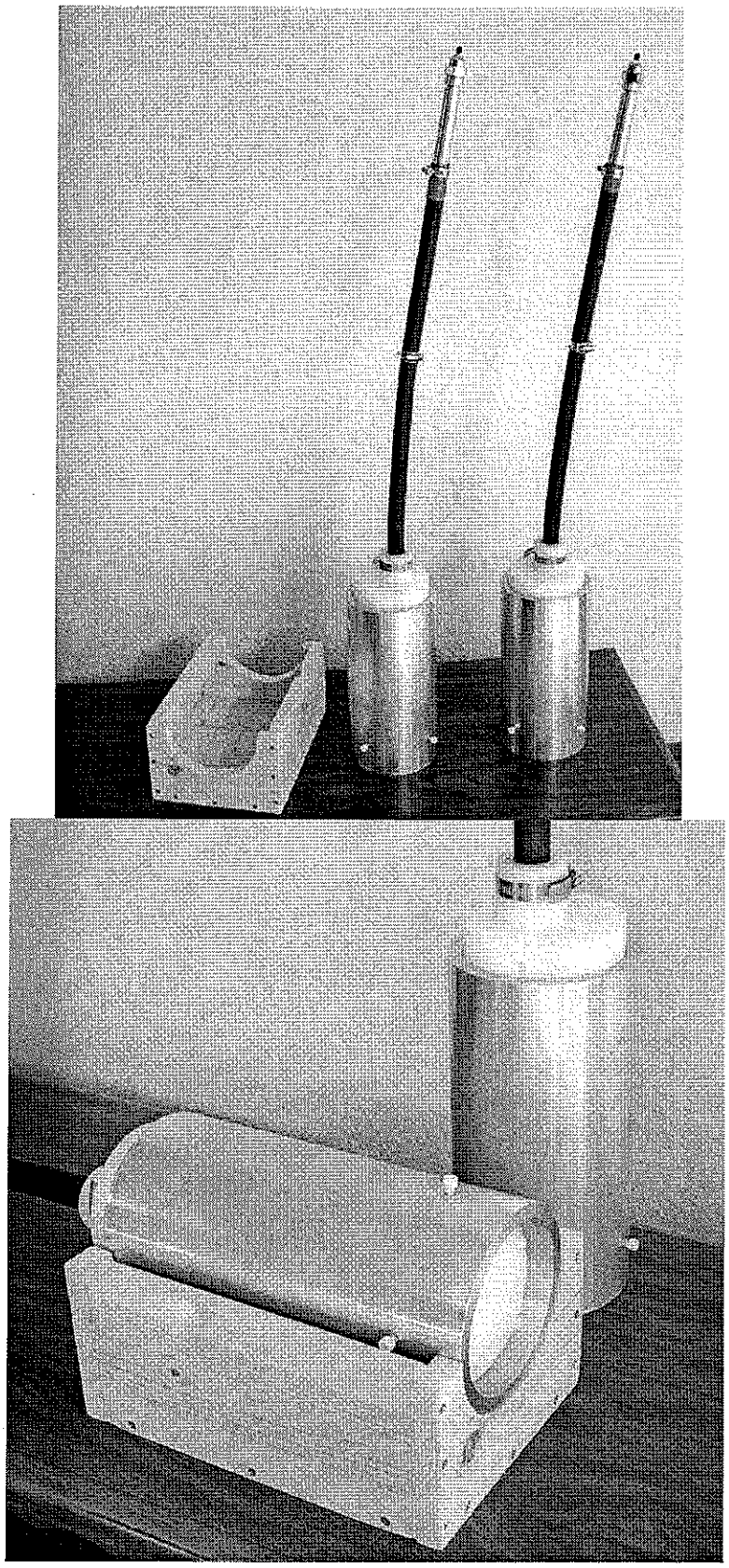

Figure 2.4. Completed SDL IRAs

In the aperture of the SDL IRAs is a lens in the shape of a prolate spheroid, or an ellipse of revolution. The lenses are fabricated from the same UHMW material as the rest of the dielectric enclosure. The SDL IRAs are fed by an RG-220 cable, which can sustain high voltages. Located about half way on the RG-220 cable is an SMA sensor designed to monitor a high-voltage drive pulse.

2.2 Dielectric Material Selection

We provide detail here on how we chose the dielectric material that fills our antennas. Our primary selection criteria were high dielectric-strength and machinability. We found several potential materials meeting these criteria and with a wide range of dielectric constants. These materials and calculated parameters for our plate design are summarized in Table 2.1.

Table 2.1. Dielectric Material Properties and Calculated Gain.

Material	Dielectric Constant	Dielectric Strength (V/mil)	*b/a* for 50 Ω	Gain due to increased aperture(dB)	Transmission Coefficient at interface	Loss due to reflection (dB)	Net gain (dB)
Air	1.0		0.17	0.00	1.00	0.00	0.00
UHMW	2.3	2280	0.27	1.9	0.80	2.00	–0.10
Tefzel	2.5	1800	0.29	2.2	0.78	2.22	–0.05
CPVC	3.7	1250	0.38	3.1	0.68	3.30	–0.19
Macor	6.0	1000	0.55	4.2	0.58	4.75	–0.60
Kynar	8.5	1700	0.70	4.6	0.51	5.84	–1.22

Based on this data, we consider now the best choice for filling the SDL IRA. There are four considerations: high-frequency performance, low-frequency performance, dielectric strength, and machinability. Dielectric strength is rather straightforward, and the numbers show that UHMW polyethylene is preferred. UHMW is also very machinable.

Next, we consider high-frequency performance of the dielectric material. In the table we list the *b/a* necessary for 50-ohm impedance between two plates for the listed dielectric material. Here, *b* is the plate separation and *a* is the plate width. The value for *b/a* is found graphically from Figure 2.4 in [3]. With this, we calculated the dimensions of the horn aperture to fit it into a 12.7-centimeter (5-inch) diameter. We sketch for each material the resulting horn aperture in Figure 2.5. We then calculated the area between the plates, and called this the aperture area of the antenna. By this definition, higher dielectric constants lead to higher aperture areas, because the plates are spaced further apart. We then calculated the increase in gain due to the increased aperture area relative to an air dielectric, as shown in Table 2.1. Based on the aperture area, higher dielectric constants are preferable.

We next calculated the loss due to the reflection at the air-dielectric interface, as shown in Table 2.1. This effect tends to favor lower dielectric constants, as shown in the table. Finally, we combined the two numbers into a net gain for high-frequency antenna performance. These calculations suggest that a low dielectric constant performs better at high frequencies.

On the other hand, at low frequencies there is an advantage in using higher dielectric constants, as shown in the following section. Ultimately, for the purposes of this investigation, we chose UHMW because it is readily available, relatively inexpensive, easily machinable, and it has the highest dielectric strength. It may well be worthwhile to try building a version with a higher dielectric constant in the future to test for better low-frequency performance.

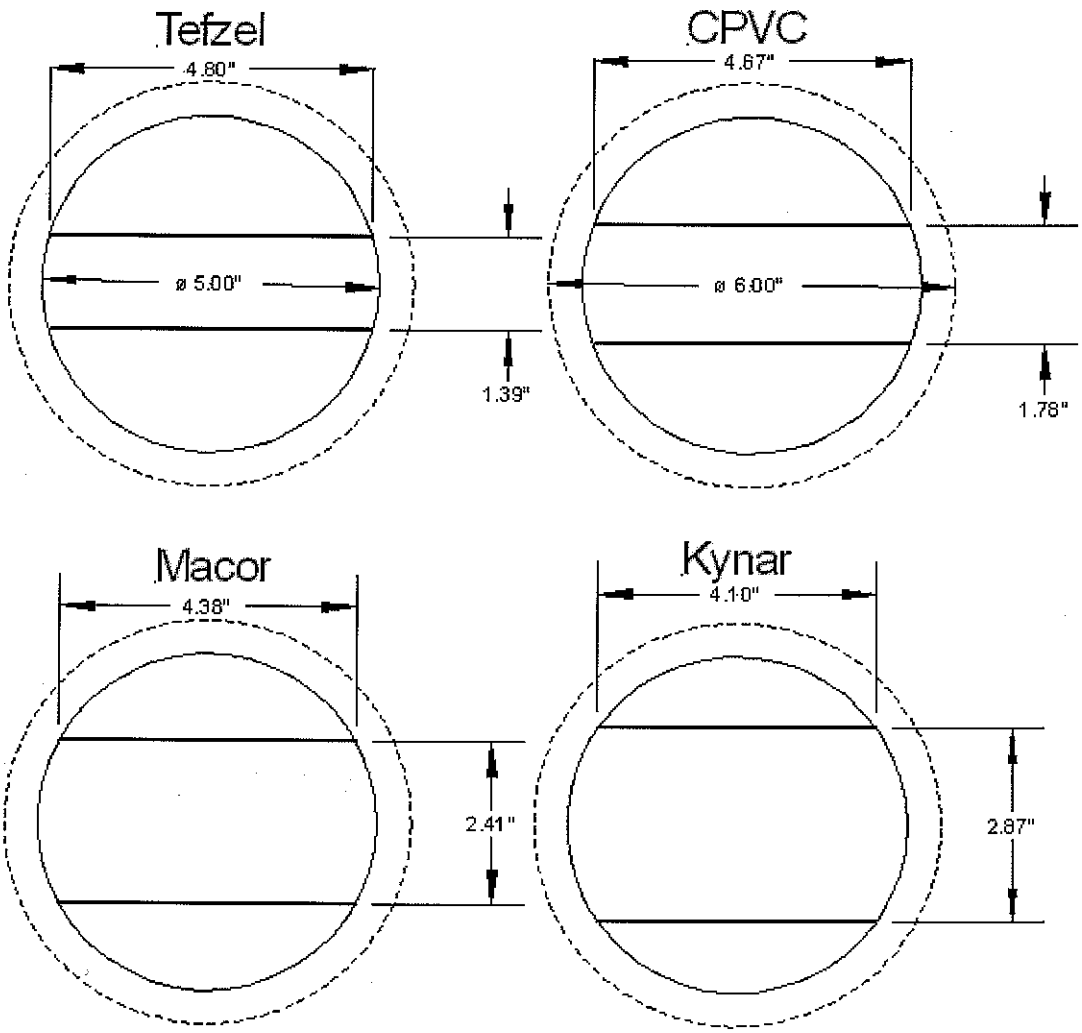

Figure 2.5. Plate size and spacing for selected dielectric materials yielding a 50-ohm impedance.

2.3 Length Considerations

We chose 20.3 cm (8 inches) for the length of the horn section of the antenna. There is an inverse relation between the length of the antenna and the low end of the low-frequency rolloff. The low end of the frequency response extends down to a frequency, f_L, which is calculated as

$$f_L = \frac{c}{2\pi\sqrt{\varepsilon_r}\,L} \tag{1}$$

where L is the length of the TEM horn, ε_r is the dielectric constant of the filling material, and c is the speed of light in free space. This expression is derived from [4, Equation 4.4], with a modification to include the effect of the dielectric material. Note that there is an apparent advantage in using a high dielectric constant for low-frequency performance. According to this expression, our antenna with a 20.3 cm length and dielectric constant of 2.25 has a low-frequency cutoff frequency of 157 MHz. This may be an optimistic prediction, since the measured data we present later in this paper show somewhat higher cutoff frequencies.

2.4 High Voltage Considerations

Of the materials considered, UHMW polyethylene has the highest dielectric strength. We rolled the edges of the TEM horn to avoid the high-field enhancements there. The rolled output edge is visible in drawings of Figures 2.1 and 2.2. All edges are polished.

The minimum spacing between the plates is 0.51 mm (0.020 in). This gives us a voltage standoff of 45 kV, calculated using a low-frequency dielectric strength of 2.28 kV per mil for the UHMW. This is a conservative estimate for fast pulse applications, since the standoff calculations assume a dc voltage.

We chose RG-220 to feed the SDL IRA. The RG-220 cable has a 14-kV DC operating voltage, and we have previously used it for fast transients with peak voltages of around 120 kV.

To allow us to measure the high-voltage source driving the antenna, we built into the feed cable a customized V-dot sensor, or so-called "SMA sensor" [5]. This sensor, shown in Figure 2.6, is simply an SMA receptacle with the center stud and insulation machined to a height of approximately 0.51 mm (0.020 in). In this case the connector is a Suhner model 23 SMA-50-0-03. The center conductor and insulation extend 0.51 mm so that it can protrude through a circular gap in the cable braid. The sensor is held in place on the feed cable by a hose clamp with a hole drilled to receive the SMA female connector.

The center stud forms a capacitively coupled pickoff from which the input signal can be reconstructed simply by integrating the sensor output and multiplying by a scalar. This scalar is determined by calibrating the sensor with a known input step. A typical calibration factor for this sensor is 3×10^{12} V/V-s.

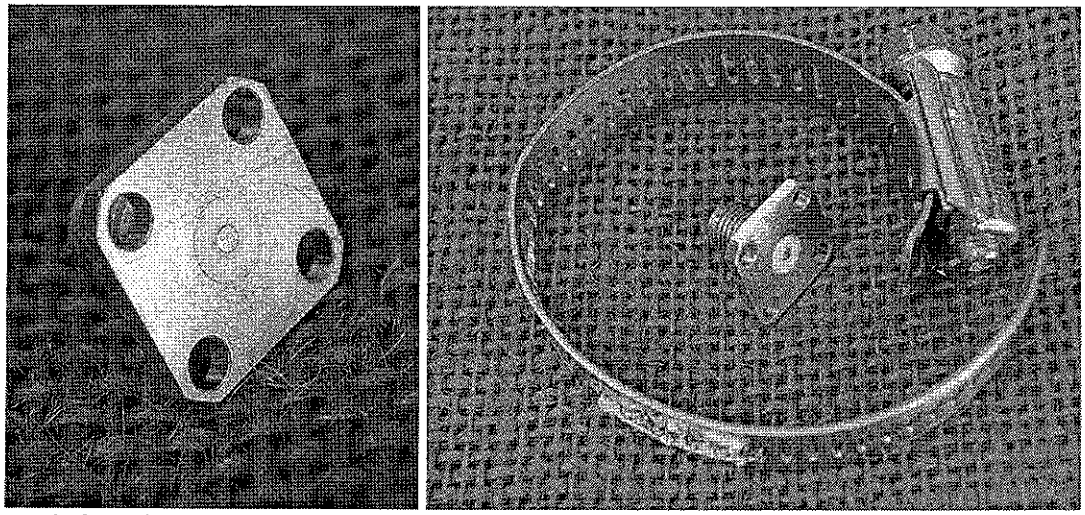

Figure 2.6. Left: SMA connector modified to form a sensor. Right: Sensor and hose clamp.

2.5 Lens Design

The design calculations for the SDL IRAs lenses come from [1]. The lens is an ellipse of revolution with a major axis of $2a$ and a minor axis of $2b$ where

$$a = \frac{L}{1 + \frac{1}{\varepsilon_r}} \tag{2}$$

$$b = L\sqrt{\frac{\sqrt{\varepsilon_r} - 1}{\sqrt{\varepsilon_r} + 1}} \tag{3}$$

and

$$\frac{b}{a} = \sqrt{1 - \frac{1}{\varepsilon_r}} \tag{4}$$

Furthermore, L is the distance from the feed point to the end of the lens and ε_r is the relative dielectric constant of the lens. Solving these equations for L, given b/a (from Table 2.1) and ε_r, yields the lens design.

2.6 Mechanical Hardening

We attempted to build an antenna that would be resistant to large forces. Our approach was to fill all voids within the antenna with UHMW polyethylene. Various ceramics and castable epoxies are candidates if the machined UHMW ultimately proves unsuitable. Additionally, there are a number of castable plastics, such as polyethylene or Rexolite, that may be suitable for the filler. Finally, there are stock dielectric materials available from microwave materials companies

such as Cuming Corp, or Emerson and Cuming Microwave Products. Our design uses a ruggedized feed point at the apex. The cable that attaches to the horn is a potential weak spot, so we completely embedded it in the UHMW material for strength.

2.7 Conducting Cylindrical Shroud

We expect that the SDL IRA will be partially shrouded by a conducting cylindrical shroud, as shown in Figure 2.7. In our design we added a metal cylinder around the TEM horn to study its effect on the radiated pulse. The shroud is a 152 mm (6 inch) outer-diameter aluminum tube with a 14 mm (0.55 inch) thick wall. The shroud and the TEM horn are entirely separate units. The TEM horn slides in and out of the shroud to any relative position for testing.

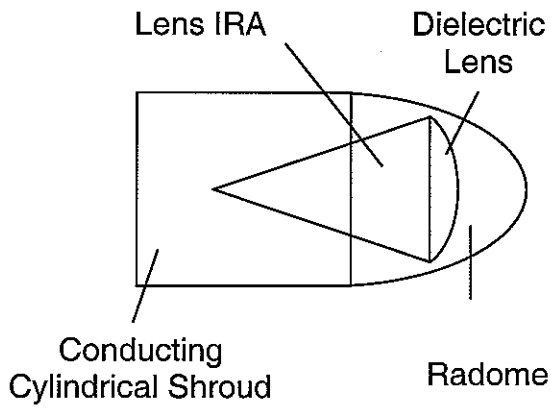

Figure 2.7. Metallic shroud surrounding the Lens IRA.

3. Farr Research Time Domain Antenna Range

We used the Farr Research time domain antenna range to characterize the SDL IRAs. The measurement system is shown in Figure 3.1. A Picosecond Pulse Laboratory (PSPL) Model 4015C pulse generator (4 volts peak, 20 ps risetime) drove a Farr Research model TEM-1-50 sensor. The SDL IRA receives the radiated pulse. A Tektronix TDS8000 digital sampling oscilloscope (DSO) with an 80E04 sampling head detects the signal. We record the data and transfer it to a desktop computer for processing.

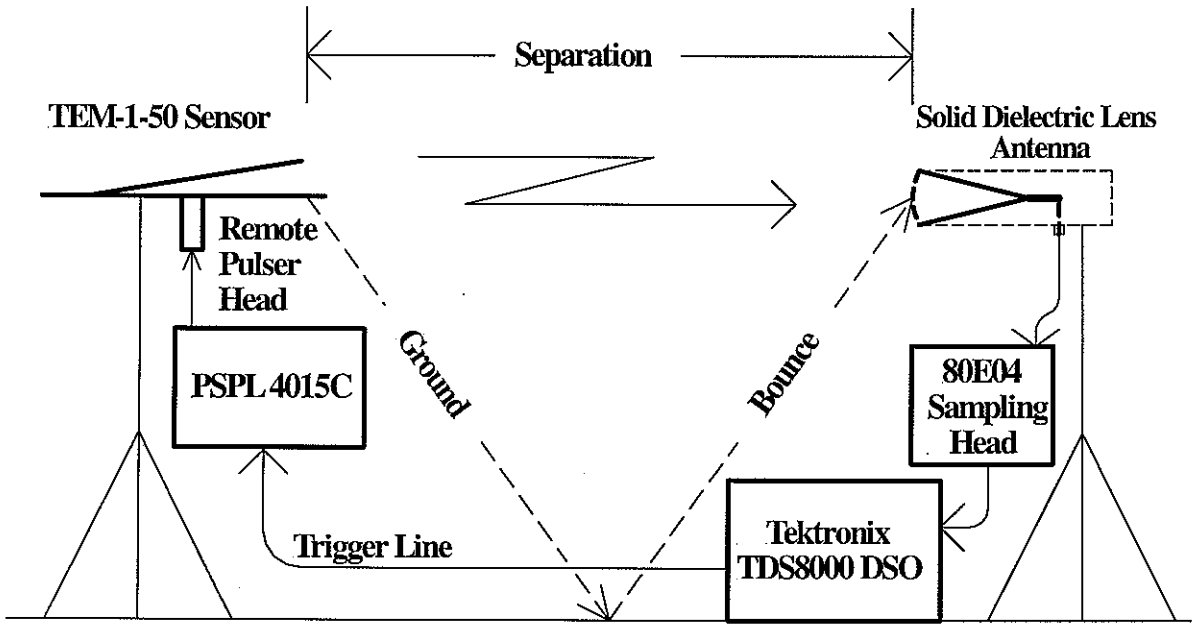

Figure 3.1. Instrumentation Setup.

4. Testing

4.1 TDR

We measured the impedance profiles of the two SDL IRAs using the TDR features of the TDS8000 and the 80E04 sampling head. Figures 4.1 and 4.2 show the impedance profiles of the two antennas with and without the shroud. Where we used the shroud it was positioned to be flush with the front of the antenna. We have superimposed a side view of the antennas aligning their physical features with the appropriate impedance discontinuities.

In both plots the input section starts with the small impedance discontinuity (from 50 ohms to about 45 ohms) near 0.6 ns on the horizontal time scale. The input section ends with the discontinuity at approximately 1.6 ns, which is also the beginning of the antenna plates. The first impedance discontinuity corresponds to the transition from the unmodified RG-220 cable to the input section, and the second from the input section to the plates.

As Figure 4.1 shows, with the cover off the 50-ohm antenna, the plates maintain the 50-ohm impedance throughout the entire length of the horn. With the cover on, the 50-ohm antenna drops to about 35 ohms until the end of the plates (at 3.7 ns) where the impedance rises to an open.

The cover affects the high-impedance version more dramatically. Figure 4.2 shows the impedance increasing to over 100 ohms with no cover. With the cover in place the impedance forms a bulge increasing from 50 ohms to 70 ohms and falling back to about 45 ohms at the end of the plate. The impedance increases with increasing plate separation but then decreases starting about midway as the plates approach the cover. Again the impedance increases to infinity at the open end of the plates.

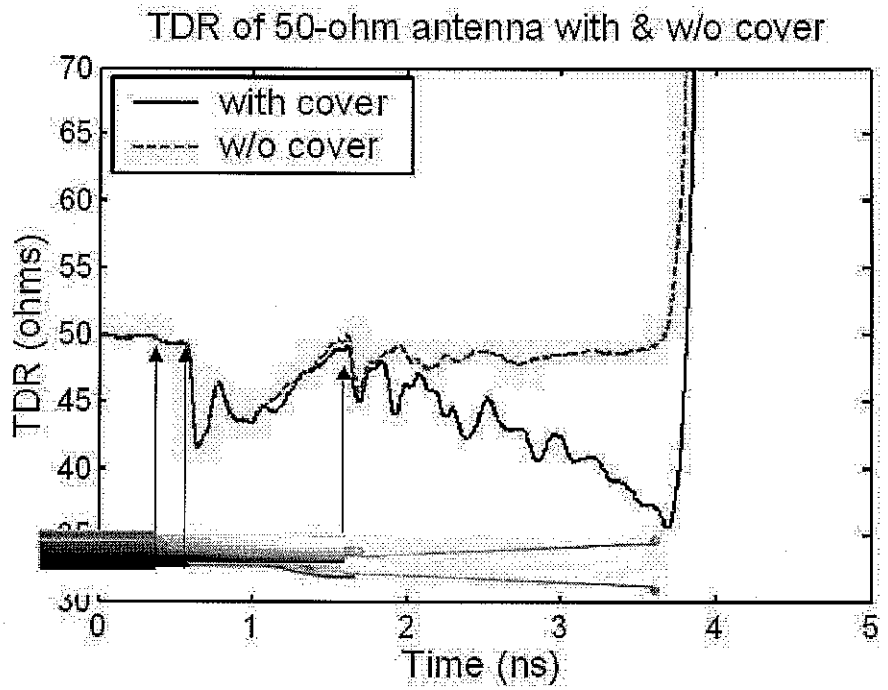

Figure 4.1. Impedance profile of 50-ohm SDL IRA.

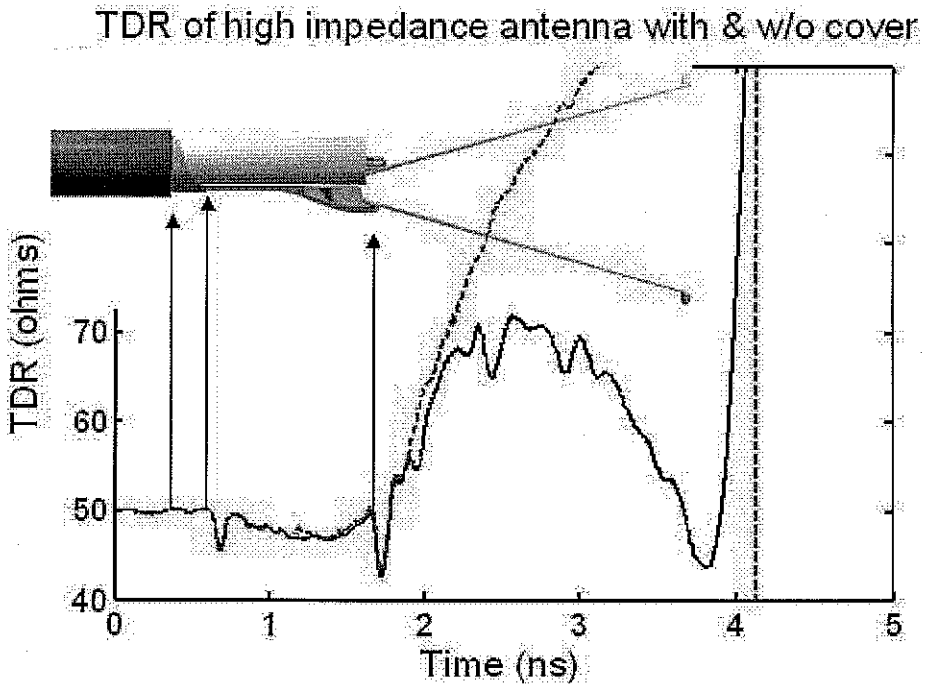

Figure 4.2. Impedance profile of high-impedance SDA.

4.2 Far Field Determination

To accurately measure the radiated field of the SDL IRAs we must ensure that we are in the far field of the radiation pattern. The far field region begins at a distance R from the horn, where three conditions for R must be met [6, Equation 1-99]

$$\begin{aligned} R &> 2D^2 / \lambda, \\ R &>> \lambda, \\ R &>> D. \end{aligned} \tag{5}$$

Here, D is the aperture diameter and λ is the wavelength. For a given R, the first equation determines the high-frequency limit of the measurements, and the second equation determines the low-frequency limit. For our antenna, the third equation is easily satisfied.

We were able to measure conveniently at a distance of 4.1 meters, so we calculate here the frequency range over which our results are valid. The aperture diameter, D, was 12.7 cm (5 inches), so this allowed a maximum frequency (by the first equation) of 38 GHz, which is well beyond the high end of our measurement capability – about 20 GHz. The second equation restricts the low end of the frequency range to 730 MHz, under the conservative assumption that the symbol ">>" means "at least 10 times greater than." So our measurements are valid over the frequency range of

$$730 \text{ MHz} < f < 20 \text{ GHz},$$

and it could be argued that they are valid even lower with a less restrictive interpretation of the ">>" symbol.

4.3 Boresight Properties of the 50-ohm SDL IRA

Next, we measured the boresight antenna properties of the 50-ohm SDL IRA. The shroud was flush with the front of the antenna and the lens was in place. We measured the realized gain on boresight, as shown in Figure 4.3 on linear and log frequency scales. The realized gain of the 50-ohm version is an essentially flat 0 dB over a broad band. We also measured the normalized antenna impulse response, as shown in Figure 4.4 and its integral, as shown in Figure 4.5. Note that the impulse response has a large overshoot to it, which detracts somewhat from the ideal impulse that is our goal.

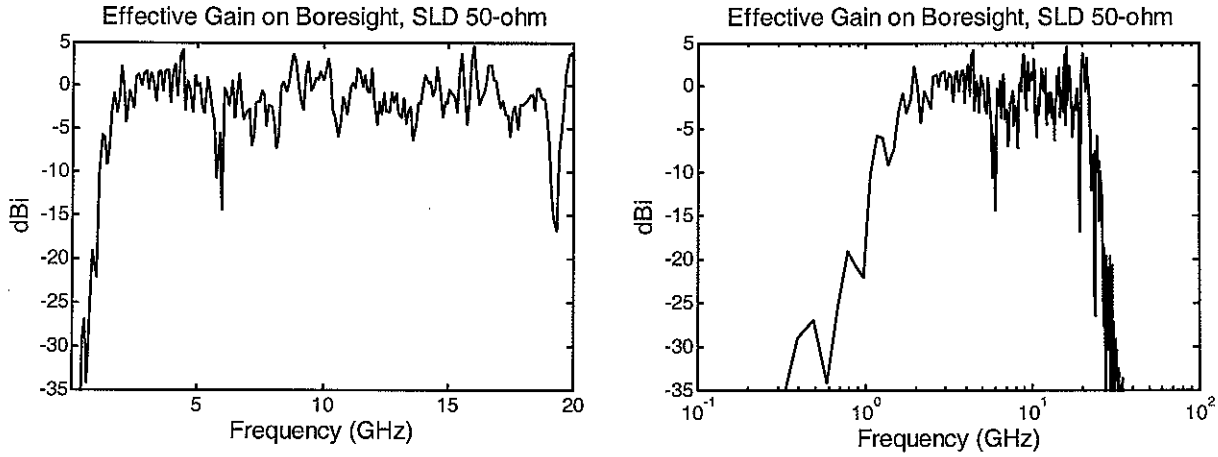

Figure 4.3. Realized gain of the 50-ohm SDL IRA.

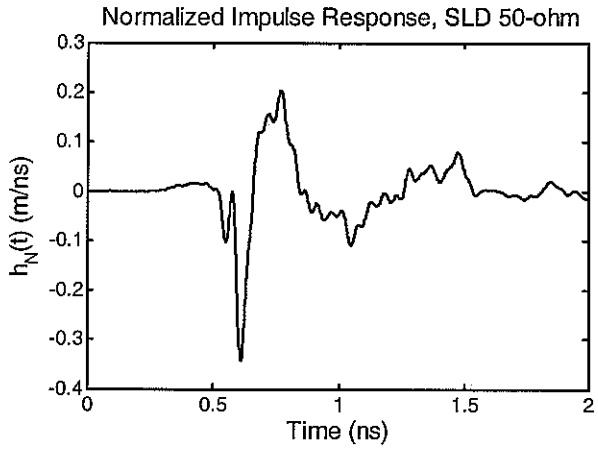

Figure 4.4. Normalized impulse response of the 50-ohm SDL IRA.

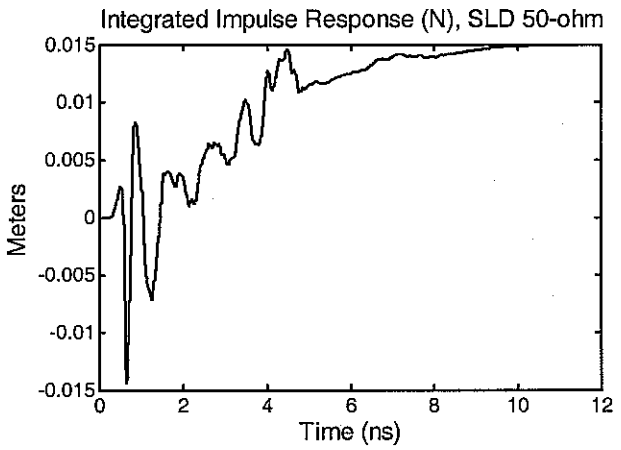

Figure 4.5. Integrated impulse response of the 50-ohm SDL IRA.

4.4 Boresight Properties of the High Impedance SDL IRA

Next, we measured the boresight properties of the high-impedance SDL IRA. The shroud was flush with the front of the antenna and the lens was in place. The realized gain is shown in Figure 4.6. The high-impedance version has better realized gain at low-frequencies, but it also has a pronounced null around 8 GHz. We also measured the normalized antenna impulse response and its integral, in Figures 4.7 and 4.8.

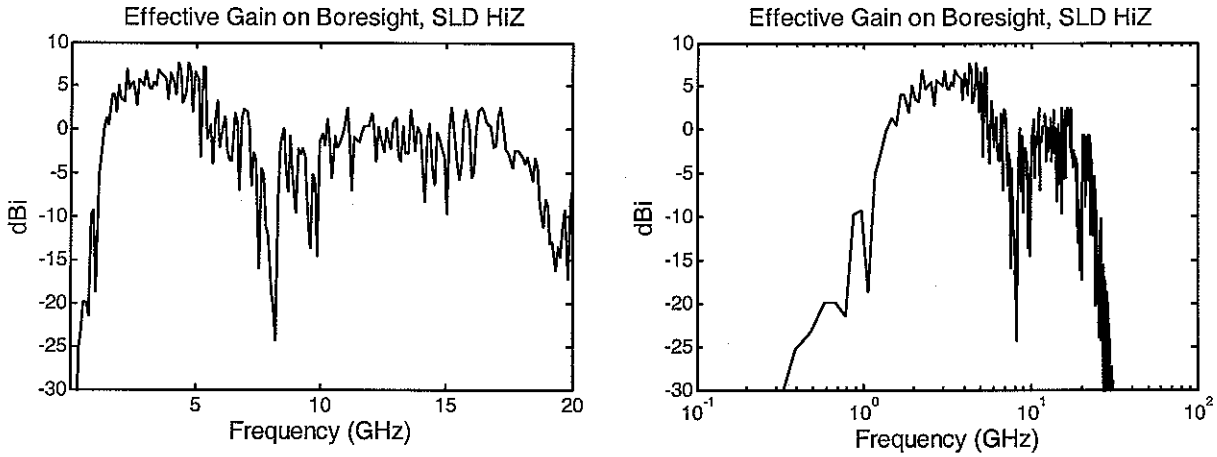

Figure 4.6. Realized gain (a.k.a. effective gain) of the high-impedance SDL IRA.

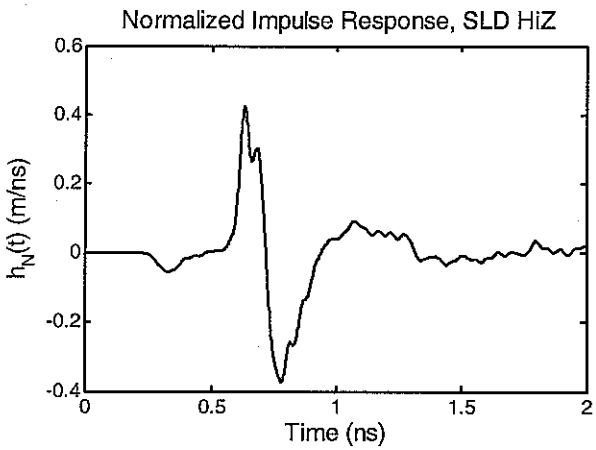

Figure 4.7. Normalized Impulse Response.

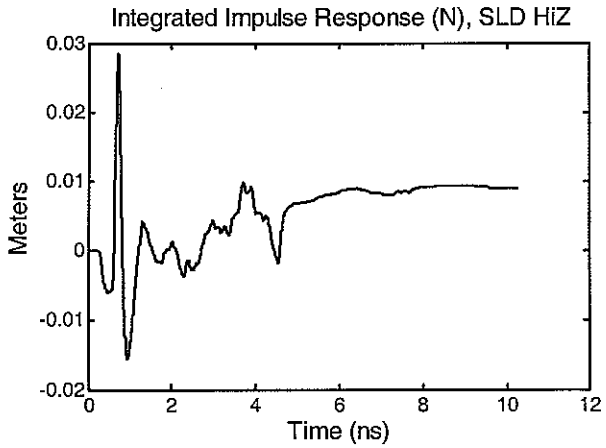

Figure 4.8. Integrated Impulse Response.

4.5 The Effect of Shroud Placement

Next, we studied the performance of the SDL IRA as we varied the position of the cylindrical shroud with respect to the antenna. First we extended the high-impedance TEM horn 10 centimeters in front of the front of the shroud. We then moved the horn back in 5-centimeter steps until it was recessed by 10 centimeters inside the shroud. This gave us a total of five measurement positions.

We present the normalized antenna impulse response for the five positions in Figure 4.9. The largest (left-most) impulse response in the figure is with the front of the antenna protruding 10 centimeters in front of the shroud. Each successive plot moving to the right is the result of a 5-cm movement of the antenna back into the shroud, until the front of the antenna was recessed 10 centimeters inside the shroud. From this time domain data, we can clearly see the advantage of having the front of the antenna protrude as far as possible in front of the shroud.

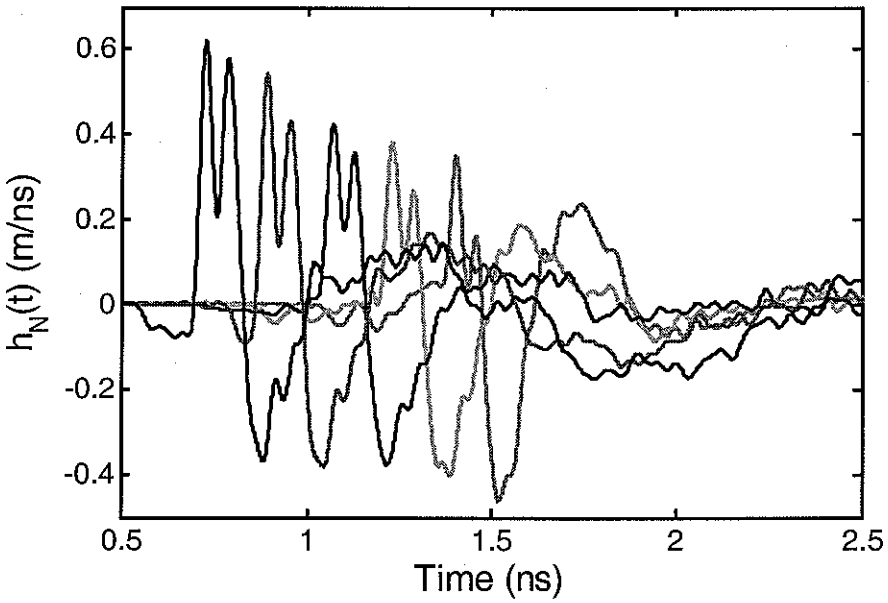

Figure 4.9. Normalized impulse response as antenna plates moved in 5 cm steps.

Next, we converted the above data to the frequency domain. This allowed us to study the effect of the antenna protrusion on the realized gain. In Figure 4.10 we plot just two of the cases: with the front of the SDL IRA protruding 10 cm, and with the front of the antenna flush with the front of the shroud. The results provide a dramatic illustration of the effect of the antenna protrusion. When the antenna protrudes the shroud by 10 cm the low-end frequency range of the antenna is around 400 MHz. On the other hand, when antenna is flush with the shroud, the low end of the antenna response is around 1 GHz. Clearly, there is a large incentive to have the antenna protrude as far forward of the shroud as possible. Note also that in Section 4.2 we estimated that our antenna range was only valid down to 730 MHz using the strictest interpretation of the ">>" symbol, so there is some uncertainty at the low end of these measurements.

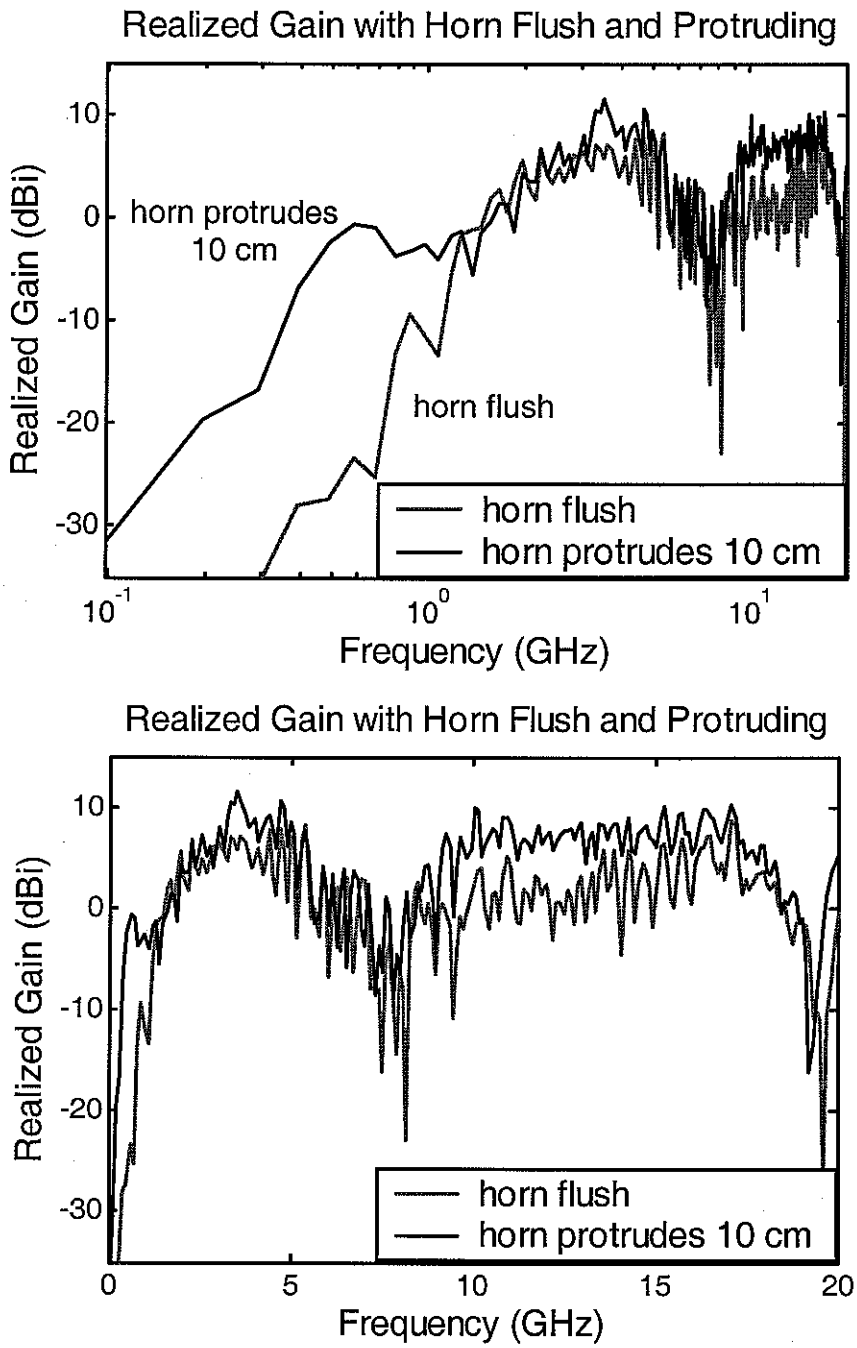

Figure 4.10. The effect of having the high-impedance version of the SDL IRA protrude from the end of the shroud on a logarithmic (top) and linear (bottom) frequency scale.

4.6 The Effect of the Lens in the High-impedance SDL IRA.

Next we measured the effect of the lens on the impulse response of the SDL IRAs. We tested the high-impedance version with the shroud flush to the antenna, both with and without the lens. The normalized antenna impulse responses for both conditions are presented in Figure 4.11. The data demonstrate that the presence of the lens is necessary to obtain optimal high-frequency performance. The lens essentially doubles the amplitude of the impulse response.

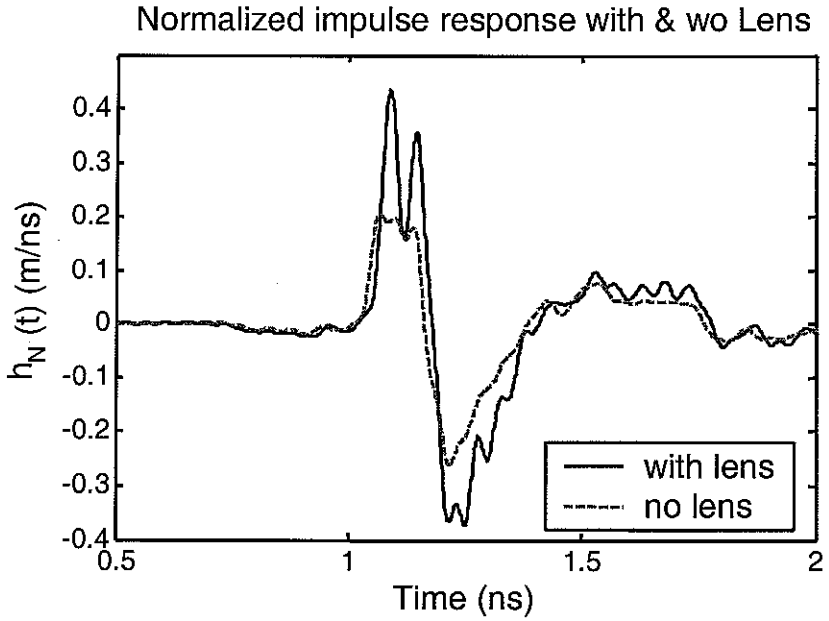

Figure 4.11. Impulse response of the high-impedance SDL IRA, lens comparison.

4.7 Terminating Resistor Placement

Next we studied the effect of the placement of the terminating resistors. We need resistors at the end of the antenna to protect the high-voltage Marx generator against reflections returning from the open-circuited horn. In-phase reflections could overvolt the Marx causing permanent damage. Resistors will absorb much of the energy not actually radiated.

Two positions for the terminating resistors are possible, as shown in Figures 4.12 and 4.13. In configuration 1 (Figure 4.12) two resistors, of approximately twice the output impedance of the plates, are placed in parallel directly across the plates of the horn. This placement shorts out some of the radiated field. In configuration 2 (Figure 4.13), two resistors, of approximately half the impedance of the plates at the output, are connected in series from the plate to the shroud. Neither plate is connected to the shroud except through these resistors.

We measured the radiated field from the two configurations with the resistors in place, and with the resistors removed. The normalized antenna impulse responses for all three configurations are shown in Figure 4.14. The resistors across the radiating face of the antenna (configuration 1) reduce the impulse response considerably. The resistor placement outside the radiating face (configuration 2) has little effect on the impulse response.

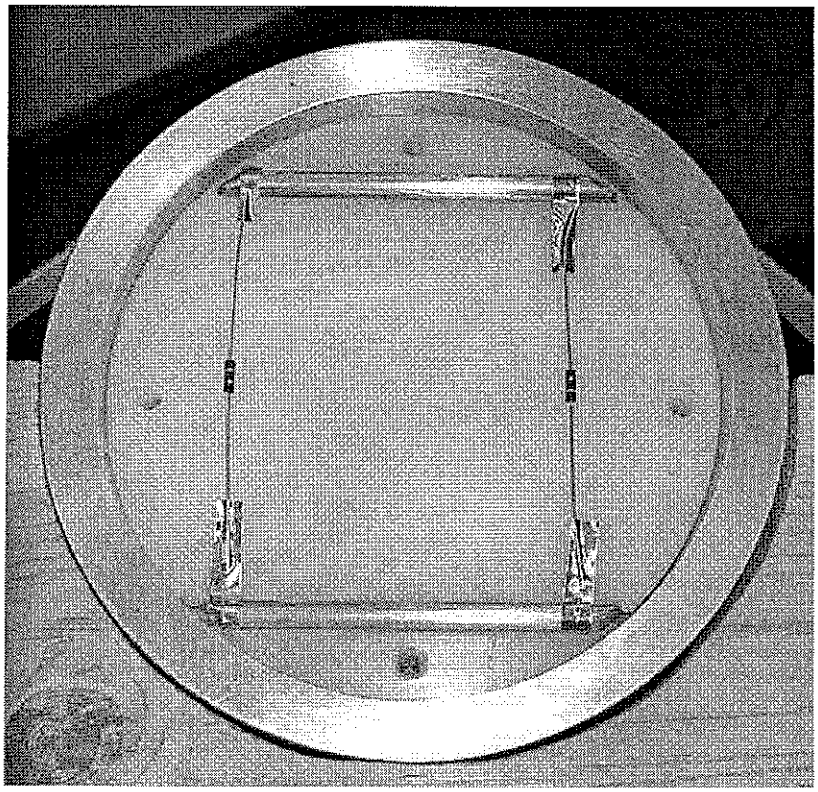

Figure 4.12. Configuration 1, with resistors across the plates of the horn.

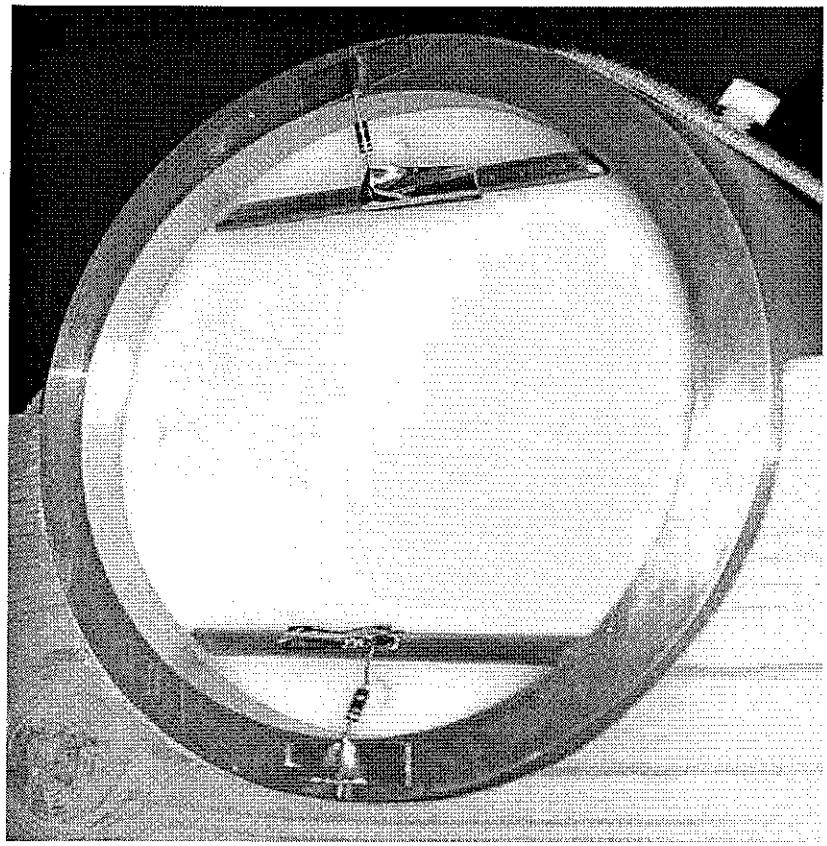

Figure 4.13. Configuration 2, with resistors connected to the shroud.

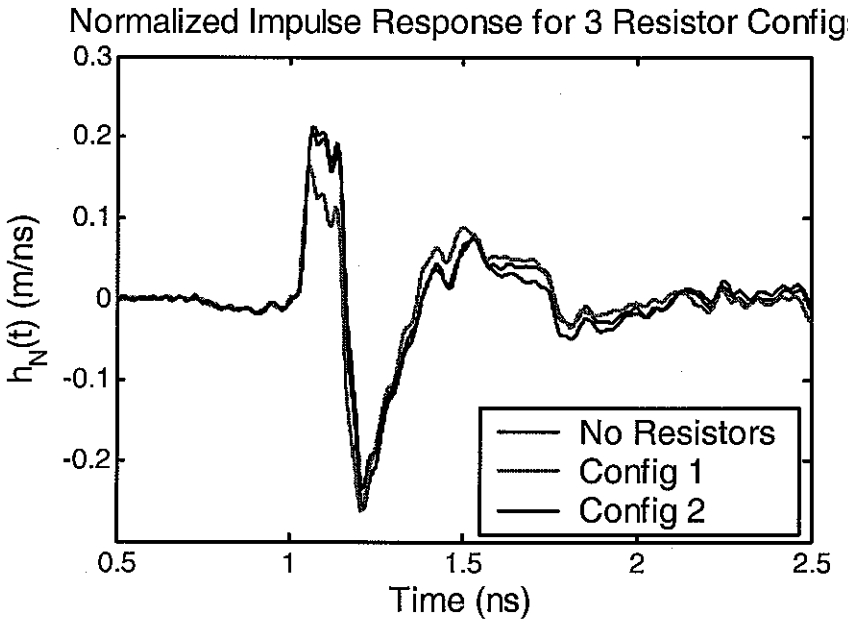

Figure 4.14. Impulse Response without terminating resistors compared to two configurations with resistors.

Finally, we note another disadvantage of connecting the resistors across the plates of the horn. With this configuration the low-frequency fields will be directed backward, instead of forward, as shown in [7,8]. To radiate the low-frequency fields forward, one needs to feed the resistors back toward the feed point. Normally the SDL IRA will protrude somewhat from the shroud, so by attaching the resistors to the front lip of the shroud we force the low-frequency fields to radiate forward.

4.8 Antenna Pattern and Beamwidth

We measured the antenna pattern and beamwidth of the high-impedance SDL IRA in both the E-plane and H-plane. We measured the pattern for the H-plane from boresight to approximately +25.7 degrees. For the H-plane we simply reflected across boresight in our calculations, based on the symmetry of the antenna. For the E-plane, there is some asymmetry in the feed section, so we measured over a range of 20° to either side of boresight.

First, we present the E-plane patterns based on both the raw voltage and the normalized antenna impulse response. Figures 4.15 and 4.16 show the E-plane patterns calculated both ways. The data demonstrate that the antenna pattern points slight up (positive angle from boresight) by approximately three degrees.

Next, we present the H-plane patterns calculated by both methods, as shown in Figures 4.17 and 4.18. The raw voltage patterns show that the 3-dB beamwidth in the E-plane is greater than 40 degrees, and in the H-plane is greater than 50 degrees. Wide beamwidth is expected with the relatively low gain of these particular horns.

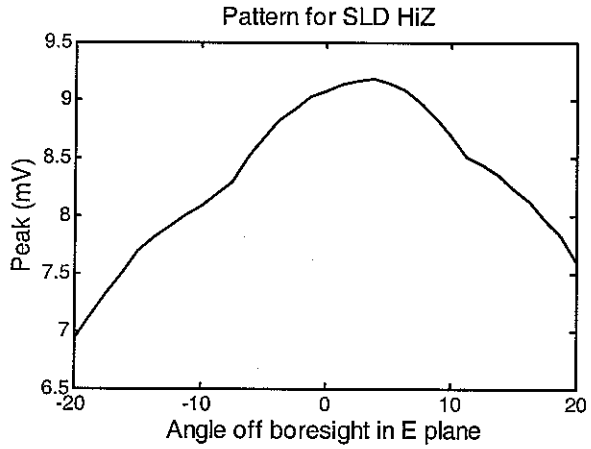

Figure 4.15. Raw voltage pattern E-plane

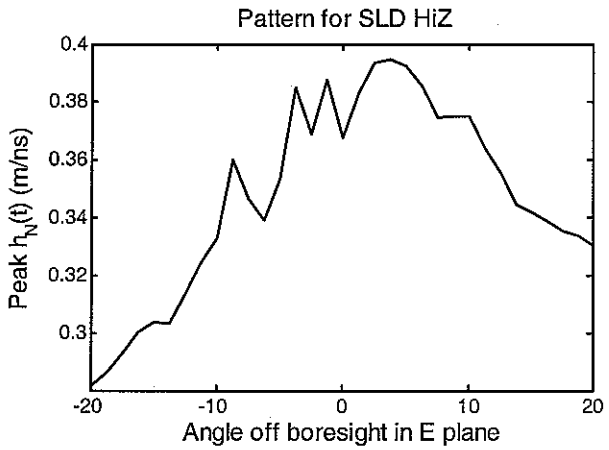

Figure 4.16. Impulse response pattern E-plane.

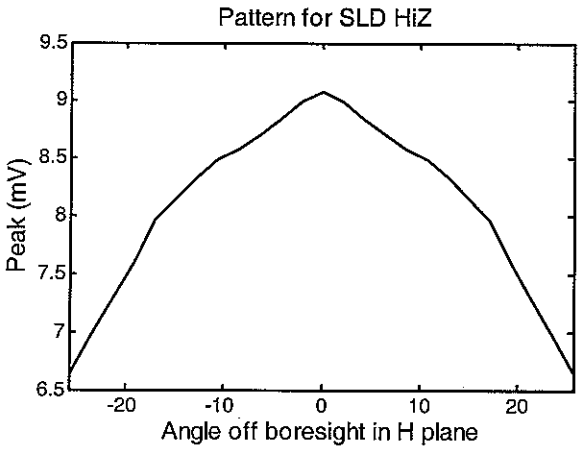

Figure 4.17. Raw voltage pattern H-plane

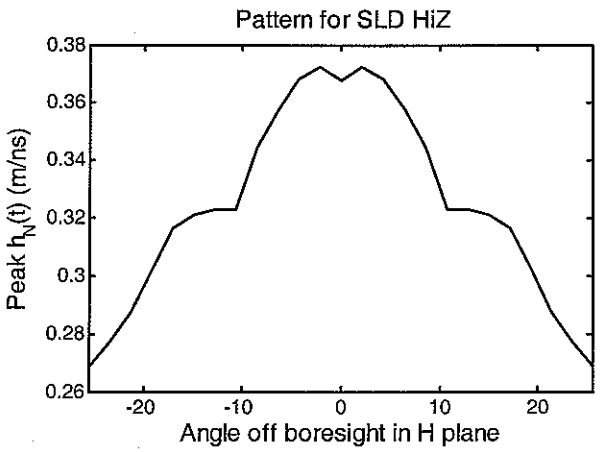

Figure 4.18. Impulse response pattern H-plane.

4.9 Gain vs. Frequency and Angle

In Figures 4.19 and 4.20 we present the realized gain in dB plotted as a color scale over frequency and angle off boresight in both the E- and H-planes. Each figure represents the entirety of the antenna gain in a single frequency- and angular-dependent plot. The patterns on the left are normalized to the boresight values, while those on the right are absolute values.

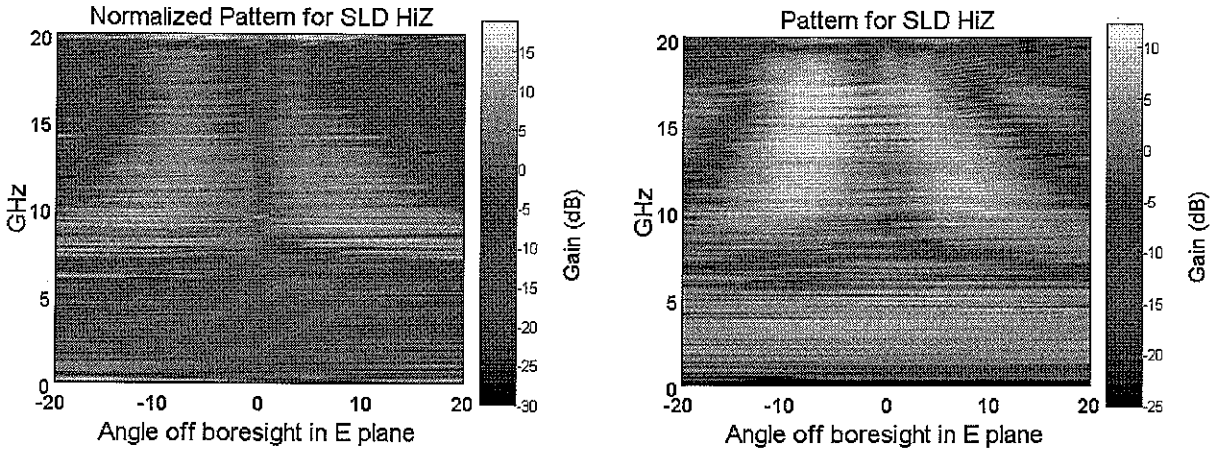

Figure 4.19. Gain as a function of frequency and angle in the E-plane.

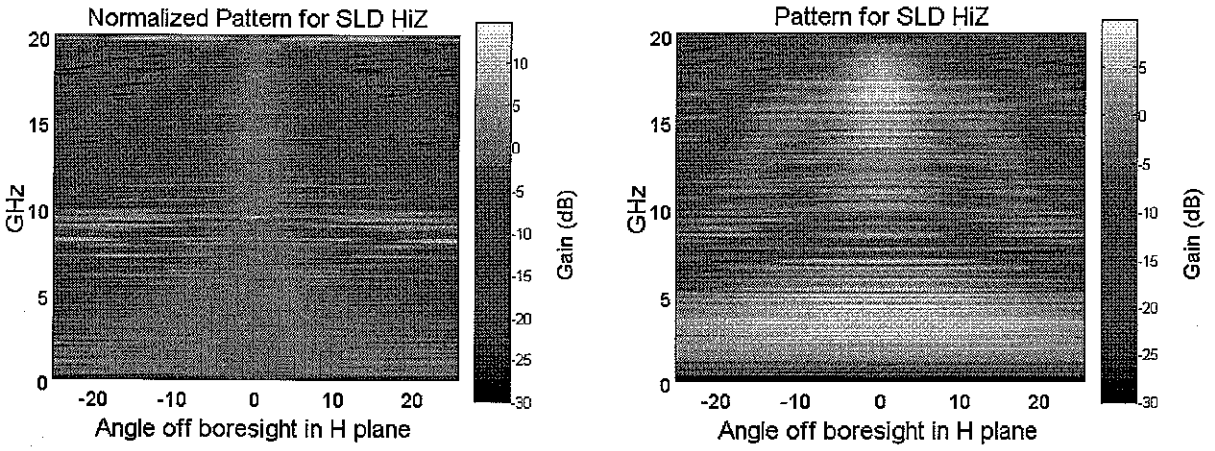

Figure 4.20. Gain as a function of frequency and angle in the H-plane.

5. Conclusions

We have built and tested two Solid Dielectric Lens Impulse Radiating Antennas (SDL IRAs) that were designed to fit within the front end of a conducting cylindrical shroud. These antennas are similar to lens TEM horns that are embedded in a solid dielectric material. In one design, we attempted to maintain a 50-ohm impedance throughout the horn all the way out to the aperture. In the second version, we allowed the impedance to increase within the horn, in order to better take advantage of the available aperture. The high-impedance version of the antenna seems to work best, providing the best impulse response. However, the 50-ohm version may be needed in applications that are sensitive to internal reflections.

The nominal frequency range of the antenna is about 400 MHz to 8 GHz when the high-impedance version of the antenna protrudes 10 cm in front of the shroud. When the antenna is flush with the shroud the low-end frequency limit is only as low as 1 GHz, so there is a large incentive to have the antenna protrude as far as possible in front of the shroud. The high-end frequency limit of 8 GHz is created by a spurious null in the spectrum, which could be removed with further experimentation. This should allow this design to reach 20 GHz, based on previous results [2].

Concerning the placement of the terminating resistors, we found it preferable to connect them from each plate to the shroud. Connecting the terminating resistors across the aperture from one plate to the other reduced the impulse response substantially. Note, however, that this test was performed with the antenna flush with the shroud, and should be repeated with the antenna protruding in front of the shroud. We also found it important to include the lens in the aperture, to maintain optimal response.

Our future work on this antenna would include a number of areas. First, we would evaluate how far forward it is reasonable to push the aperture of the antenna beyond the shroud, in order to optimize performance. Next, we would investigate how to smooth out some of the rough spots in the TDR to reduce internal reflections and to eliminate the null at 8 GHz. We would also test the design for high voltage and high mechanical forces. In addition, we would experiment with replacing the UWMW polyethylene dielectric with a material with a higher dielectric constant. We hypothesize that this should help the low-frequency response, because the antenna would be effectively larger.

Other areas worth exploring in future work concern the details of the aperture. We note that the fields immediately above the top plate and below the bottom plate have the incorrect orientation. So we should obtain a somewhat improved early-time response if we block these out by attaching conducting "lips" to the ends of each plate of the horn. Finally, we note that previous versions of this antenna used curved plates that followed the surface of a circular cone [1,2]. Such designs take better advantage of the available aperture area, but they also exacerbate the flashover problem at the edge of the plates. Thus, some experimentation will be needed to determine the optimal compromise.

References

1. E.G. Farr and C.A. Frost: Development of a Reflector IRA and a Solid Dielectric Lens IRA, Part I: Design, Predictions, and Construction, Sensor and Simulation Note 396, April 1996.

2. E. G. Farr and C. A. Frost, Development of a Reflector IRA and a Solid Dielectric Lens IRA, Part II: Antenna Measurements and Signal Processing, Sensor and Simulation Note 401, October 1996.

3. E.G. Farr, Optimization of the Feed Impedance of Impulse Radiating Antennas Part II: TEM Horns and Lens IRAs, Sensor and Simulation Note 384, November 1995.

4. E. G. Farr and C. E. Baum, A Simple Model of Small-Angle TEM Horns, Sensor and Simulation Note 340, May 1992.

5. E. G. Farr, L. M. Atchley, D. E. Ellibee, W. J. Carey, and L. L. Altgilbers, A Comparison of Two Sensors Used to Measure High-Voltage, Fast-Risetime Signals in Coaxial Cable, to appear shortly as a Measurement Note.

6. W. L. Stutzman and G. A. Thiele, Antenna Theory and Design, Second Edition, Wiley, 1998.

7. M. H. Vogel, Design of the low-Frequency Compensation of an Extreme-Bandwidth TEM Horn and Lens IRA, Sensor and Simulation Note 391, February 1996.

8. C. E. Baum, Low-Frequency Compensated TEM Horn, Sensor and Simulation Note 377, January 1995.